Experimental Study of Aerodynamic Noise vs Drag Relationships for Circular Cylinders

James D. Revell,* Roland A. Prydz,† and Anthony P. Hays‡
Lockheed-California Company, Burbank, Calif.

An experimental program has been conducted to determine the quantitative relationship between far-field noise and drag coefficient for circular cylinders. The test program included smooth and roughened cylinders with Reynolds numbers between 45,000 and 450,000 and Mach numbers between 0.1 and 0.5. The resulting drag coefficients varied between 0.75 and 1.2. The results show a strong dependence of SPL on drag coefficient varying as 50 to 90 times log (C_D) depending on directivity angle and bandwidth. This represents the first controlled laboratory data available to directly verify the quantitative relationship between noise and drag coefficient at constant Mach numbers.

Nomenclature

a_0 = speed of sound in freestream, m/s
a_F = constant in linear regression analysis of Mach corrected far-field SPL vs $\log_{10}C_D$, dB [Eq. (9)]
b = span of cylinder, m
b_F = slope of the regression line of Mach corrected far-field SPL vs $\log_{10}C_D$, dB [Eq. (9)]
C_D = drag coefficient of cylinder (as measured)
C'_D = (1.2/1.3) X C_D; normalized drag coefficient for 1.9-cm cylinder data
C_{p_s} = $(p_L - p_0)/q$; local surface static pressure coefficient
d = cylinder diameter, m
D = aerodynamic drag on cylinder, N
DI = directivity index of cylinder noise, dB
f = frequency, Hz
k = grit or roughness particle size, cm
$k = \omega/a_0$ = acoustic wave number, 1/m
L = lift force, N
$\overline{LD}$ = cross correlation of lift and drag, N^2
l_x, l_y = (streamwise, spanwise) surface pressure correlation lengths, m
M = Mach number
N_y = number of random dipoles along cylinder span
n = velocity dependence exponent of far-field noise
OASPL = overall sound pressure level (re: 2×10^{-5} Pa)
p_0 = ambient (freestream) static pressure, Pa
p_F = far-field acoustic pressure, Pa [Eq. (1)]
p_{SL} = sea-level static pressure, Pa
q = $\frac{1}{2}\rho_0 u_0^2 = 0.7\, p_0 M_0^2$; dynamic pressure, Pa
R = statistical correlation coefficient
r = distance from cylinder to far-field point, m
S = standard deviation from linear regression curve of Mach corrected SPL vs $\log_{10}C_D$, dB
S_Y = standard deviation from mean value of Mach corrected SPL, dB
SPL = sound pressure level (re: 2×10^{-5} Pa), dB
SPLNB = narrowband SPL (re: 2×10^{-5} Pa, for $\Delta f = 10$ or 20 Hz), dB
SPL ⅓ = one-third octave band SPL (re: 2×10^{-5} Pa), dB
St = Strouhal number fd/U_0
St_0 = reference Strouhal number, Eq. (5)
U = local streamwise velocity component, m/s
U_0 = freestream velocity, m/s
(x,y) = Cartesian coordinates in directions, respectively, streamwise and perpendicular to both cylinder axis and freestream velocity vector, m
α = exponent in St vs C_D relation, Eq. (5)
β = drag dependence exponent for surface pressure fluctuation, Eq. (3)
γ = exponent relating C_D to base pressure coefficient
θ_i = directivity angle for far-field microphones relative to upstream flow direction, deg
λ = acoustic wave length, m
ρ = fluid density, kg/m^3
ϕ = angle from stagnation point along cylinder surface, deg
ω = circular frequency, rad/s

Superscripts and Subscripts

D = drag
$\overline{(\ )}$ = mean squared value
F = far field
L = lift
TE = trailing edge (base region)
x = along freestream axis
y = along axis perpendicular to both the freestream axis and the cylinder axis

Introduction

In a series of papers over the past few years, the first author has formulated an approach to the analysis of airframe (nonpropulsive) aerodynamic noise known as the drag element method.[1-3] In this method empirical factors for prediction of the aerodynamic noise of such components as wings, flaps, landing gears, etc., have been expressed in terms of component drag coefficients. The motivation is to allow the systematic prediction of the effects of "aerodynamic cleanliness" on the aerodynamic noise radiated by general aircraft configurations, by use of aerodynamic drag data.

The methodology of Ref. 2 employed noise data from flyover tests[4-6] with estimated aerodynamic data for those aircraft. Clearly, it is desirable to have controlled laboratory tests of both drag and far-field noise for simple aerodynamic test bodies to directly evaluate the asserted quantitative dependence of far-field acoustic pressure upon drag coefficient. Such a test program was conducted by the Lockheed-California Co., under sponsorship of the NASA Langley Research Center.[7] This paper reports a brief summary of the far-field acoustic and drag data correlation from Ref. 7.

Presented as Paper 77-1292 at the AIAA 4th Aeroacoustics Conference, Atlanta, Ga., Oct. 3-5, 1977; submitted Oct. 3, 1977; revision received May 2, 1978.

Index categories: Aeroacoustics; Noise; Subsonic Flow.

*R&D Scientist, Acoustics Staff. Associate Fellow AIAA.
†Research Scientist, Acoustics Staff.
‡Research Scientist, Acoustics Staff. Member AIAA.

Theory of Noise vs Drag for a Bluff Body

The theory governing far-field noise radiated by a cylinder is classified in Ref. 2 as profile drag noise when the length to diameter is large and the flowfield about the cylinder is nearly two dimensional. Generalizing the analysis of Ref. 2, Eq. (24), a spanwise distribution of random point lift and drag dipoles is assumed and the mean squared far-field acoustical pressure can be expressed as follows:

$$\overline{p_F^2} = \frac{9}{16\pi^2 r^2}\frac{b}{l_y}\left(\frac{\omega^2}{a_0^2}\right)\{\overline{L^2}\sin^2\theta + 2\overline{LD}\sin\theta\cos\theta + \overline{D^2}\cos^2\theta\}\cos\left(\frac{\omega l_y}{a_0}\right) \quad (1)$$

Equation (1) can be further developed for bluff bodies by similarity arguments[1,2,7] to show that the far-field sound pressure is proportional to Mach number to the sixth power as is well known, but also multiplied by a factor of drag coefficient to an exponent of the order of 6, which is the focus of this paper. The key assumptions are as follows:

1) The spanwise and chordwise pressure fluctuation correlation lengths, l_x and l_y, at the trailing edge are proportional to drag coefficient times the diameter ($l_x, l_y \sim C_D d$), which, from Ref. 8, p. 621, equals twice the wake momentum thickness.

2) The rms surface pressure fluctuations in the base pressure, or trailing-edge region are proportional to the local boundary-layer edge dynamic pressure q_{TE} times the drag coefficient to an exponent β. Assumption 2 is well established for smooth and rough plates.[9]

3) The number of uncorrelated trailing-edge dipoles along the span is $N_y = b/l_y$.

4) The Strouhal frequency for vortex shedding is $f = U_{TE}(St_0/C_D^{\alpha})/d$ where α is an exponent of the order ¾ (Ref. 10).

5) The fluctuating force for each small element is proportional to the rms pressure fluctuation times $l_x l_y$.

6) The base pressure coefficient, and hence trailing-edge velocity where the flow separates, is expressible in terms of the drag coefficient for bluff bodies in the form $C_D = K_{BP}(1 - C_{PTR})^{\gamma}$.

The final expression as derived in more detail in Refs. 11 and 7 in SPL format is as follows:

$$\mathrm{SPL} = K + 60\log M_0 + DI(\theta) + 10\log(bd/r^2) + 20\log(p_0/p_{SL}) + 10(3 + 2\beta - 2\alpha + 3/\gamma)\log_{10} C_D \quad (2)$$

where the surface pressure fluctuations are defined by

$$\overline{\Delta_p^2} = K_p^2 C_D^{2\beta} q_{TE}^2 \quad (3)$$

At low Mach numbers the following approximation applies

$$q_{TE} \cong q_0[(1 - C_{p_{TE}}) + 0.25M_0^2 C_{p_{TE}}^2](1 + 0.7M_0^2 C_{p_{TE}})^{-5/7} \quad (4)$$

The Strouhal frequency is generalized from Ref. 10, pp. 3-6, as

$$f = St_0 U_0 (U_{TE}/U_0)/dC_D^{\alpha} \quad (5)$$

and the base pressure vs drag coefficient correlation

$$C_D = K_{BP}(1 - C_{p_{TE}})^{\gamma} \quad (6)$$

By choosing $\beta = 1$, $\alpha = ¾$, and $\gamma = 1$ one obtains from Eq. (2) that at a fixed microphone position,

$$\mathrm{SPL} = K_1 + 60\log M_0 + 65\log_{10} C_D \quad (7)$$

The primary purpose of this paper is to provide controlled laboratory data to support Eq. (7). For this purpose it is convenient to define Mach corrected SPL, Y as

$$Y = (\mathrm{SPL} - 60\log_{10} M_0 - 20\log p_0/p_{SL}) = Y(C_D) \quad (8)$$

The experimental data to be discussed below will show that for a given far-field location, Y is a nearly universal function of C_D for a wide range conditions, including both roughness and Reynolds number effects, thus, substantiating the preceding theory. Furthermore, the data will show that the factor 65 log C_D is a good description of the quantitative dependence upon C_D for circular cylinders. This is a stronger dependence than the 30 log C_D dependence derived for streamline bodies in Ref. 2. The difference can be attributed to Eq. (6) applicable to bluff bodies; by contrast, for streamline bodies C_{PTE} ranges from about 0.2 to 0 until flow separation is forced, for example, on a wing at high angles of attack. In the method of Ref. 2 this effect is approximately modeled by estimating the trailing-edge pressure in terms of a pressure recovery factor times the difference between stagnation pressure and the minimum pressure. In principle, the trailing-edge pressure recovery could be deduced from the methods of boundary-layer theory (Ref. 8, p. 566).

Test Facility

Acoustic and aerodynamic tests were conducted in the Lockheed-California Company Rye Canyon freejet anechoic wind tunnel to test the described drag element theory for far-field aerodynamic noise of circular cylinders. A brief description of the facility follows; more details are contained in Ref. 7. Figure 1 shows the test setup. The test section has a depth of 0.24 and a span of 0.48 m. The circular test cylinders of 1.9- and 3.8-cm-diam are of 0.48-m span and were centered in an endplate installation, which extended the shorter nozzle sidewall dimension (of 0.24-m depth) beyond the nozzle to downstream a distance of 0.448 m. The centerline of the cylinder installation is located at a distance of 0.222 m downstream from the nozzle exit. The tunnel has ratios of cylinder span to diameter of 12.7 and 25.3, respectively, for the 3.8- and 1.9-cm cylinders. Likewise, the tunnel depth to cylinder diameter ratios are respectively 6.35 and 12.70. For these conditions aerodynamic blockage effects are calculated

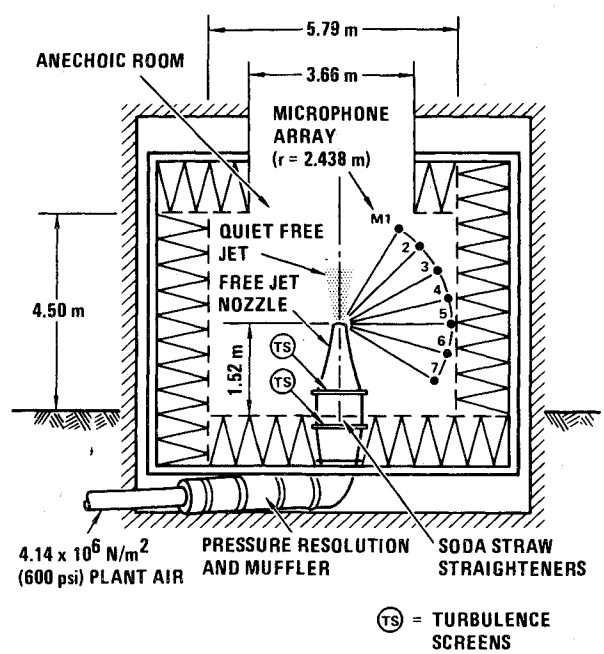

Fig. 1 Freejet test setup in anechoic chamber.

to be negligible (local velocity error less than 3% of freestream velocity for the large cylinder by use of the classical image theory of hydrodynamics). The free-jet wind tunnel discharges into an anechoic chamber having interior cross-sectional dimensions of 5.79×5.79 m, and a height of 4.50 m. The interior is lined with acoustical absorptive wedges which are 1.37-m deep, permitting good anechoic performance above 62 Hz, which is confirmed by background noise measurements.

The far-field noise measurements are recorded by an array of seven microphones on an arc of 2.44-m radius, as shown in Fig. 1. This distance represents one wavelength at a frequency of 139 Hz; therefore, all measurements above 139 Hz are valid far-field results including those measured at the lowest Strouhal frequencies tested (about 160 Hz for the 3.8-cm cylinder at $M=0.1$). The background noise level was measured and analyzed in band widths of 10 Hz, 20 Hz (hereinafter called narrowband noise), and in one-third octave bands from 50 Hz to 10,000 Hz. For the narrowband data, the minimum signal-to-noise ratio at the lowest Strouhal frequency was about 12 dB. The seven far-field microphones were spaced in 15-deg angular increments in a plane perpendicular to the wide dimension of the nozzle exit. The angular range of the far-field microphones was $\theta=60$ deg to 150 deg from the flow axis when looking upstream.

The wind-tunnel operation was of a blowdown variety with air being supplied from large remote storage tanks, pressurized to 40-atm gage pressure. The air is throttled through many valves and mufflers and eventually reaches the test nozzle with maximum stagnation pressure of about 1.75 times the ambient pressure for the present nozzle when operating at maximum flow capacity, allowing test Mach numbers in excess of 0.9 for short duration. Pumps operate to maintain tank pressure, so that continuous operation of this nozzle is possible at test Mach numbers up to 0.4. In all cases the test run time was long enough for adequate sampling of the acoustic data.

The turbulence intensity in the empty test section varied from 0.2% to 0.4% of freestream velocity for wide frequency bandwidth filter settings (0.05 to 4 kHz). However, at the lowest Strouhal frequency the turbulence intensity for the 10-Hz narrowband width was less than 0.1%. The mean flow velocity profiles are uniform within a fraction of 1% along the entire span of the cylinder, except at lateral distances near the edge of the mixing layer between the free jet and the ambient air. The acoustic background noise level is close to that predicted by standard empirical jet noise estimation techniques, confirming the expected noise floor.

The nozzle exit plane is parallel to the floor and 1.52 m above it, as shown in Fig. 1. The flow discharges vertically through the roof through a 3.66×3.66-m opening. Thus, the flow discharge area is larger than the nozzle exit area by a ratio of 116 to 1 so that "flow collector noise" discussed in Ref. 12 is eliminated. Makeup air flow is supplied through doors having 51 times the nozzle exit area, minimizing flow circulation effects within the anechoic chamber.

Experimental Program Instrumentation and Data Acquisition

Reference 7 reports extensive measurements of far-field acoustic pressure, drag coefficient, surface static pressure distribution, fluctuating surface pressure, and wake turbulence intensity for each of two circular cylinders for a wide range of test conditions. The test conditions include Mach numbers between 0.1 and 0.5 and Reynolds numbers based on diameter between 45,000 and 450,000. The test cylinder diameters are 3.81 cm and 1.905 cm.

It is emphasized that Mach number and Reynolds number are not varied independently in these tests; however, the test conditions selected were a compromise between conflicting acoustic test requirements (achieving far-field test conditions) and aerodynamic requirements to achieve high Reynolds number at low Mach numbers with large-sized cylinders. It was felt that the presence of compressibility effects in the drag data would not alter the hypothesized relationship between drag and far-field noise in the absence of shock waves; therefore, it was considered to be acceptable to allow Reynolds number and Mach number to vary together up to $M=0.5$, where for the present tests the maximum local Mach numbers were still subsonic.

Both cylinders were tested with smooth surface conditions, and also with boundary-layer transition trips installed to cause controlled variations of the drag coefficient at a given Mach number and Reynolds number. The boundary-layer transition strips (called simply BL trips hereinafter) are strips of fine, carborundrum grit particles attached to the cylinder with a thin coat of lacquer of a finite circumferential width. Two different BL trips were used for the 3.81-cm cylinder called BL trips A (75 deg$<\phi<$105 deg) and B (45 deg$<\phi<$105 deg) where ϕ is the circumferential angle from the stagnation point. The BL trip A configuration was duplicated for the 1.905-cm cylinder. Table 1 summarizes the BL trip configurations employed.

The ratio of grit particle diameter to cylinder diameter was 0.0067, yielding roughness Reynolds number between 300 and 3000. The BL trip strip technique is based on that of Braslow et al.,[13] which is commonly used for fixing laminar-turbulent transition for wind-tunnel models of aircraft wings and bodies. The purpose of using this technique here was to save time by limiting the application and removal of the grit particles to only a small portion of the surface area. By contrast, most of the existing drag data for roughened cylinders are for those having a uniform distribution of roughness particles. The present technique did succeed in the purpose of providing controlled variation of C_D with Reynolds number; however, there was some lack of repeatability, leading to the designations of BL trips AA and BB, respectively, for the repetitions of BL trips A and B as described in Table 1. Figure 2 shows the BL trip configurations, the surface static pressure tap locations, and the Kulite CQ-080-5 transducer at $\phi=120$ deg.

The far-field acoustic data acquired for each test condition consisted of one-third octave band sound pressure levels (SPL), for each of seven microphones. Narrowband SPL data analyses were conducted for microphone 5 at $\theta_i=90$ deg, using the Hewlett Packard HP-5451B Fourier analyzer, employing 250 line spectra over a frequency range of 2.5 kHz, for the 3.81-cm cylinder, and to 5 kHz, for the 1.9-cm cylinder, providing bandwidths of 10 Hz and 20 Hz, respectively. The surface pressure fluctuations as measured by the Kulite transducer, designated as microphone 8, were also subjected to similar narrowband and one-third octave band analyses. The surface pressure fluctuation data are contained in Ref. 7, but are omitted here for brevity.

The aerodynamic drag data presented herein were obtained by integrating the product of pressure coefficient times $\cos\phi$ around the circumference. For bluff bodies, this procedure is acceptable since friction drag is negligible for the present test Reynolds number range (Ref. 14, Vol. II, p. 425).

Table 1 Boundary-layer trip configurations

Diameter, cm	BL trip configuration	Angular range, deg	Mean grit size (k)-cm	k/d	Grit no.
3.81	A, AA	75 to 105 −75 to −105	0.0254	0.0067	60
	B, BB	45 to 105 −45 to −105	0.0254		
1.905	A	75 to 105 −75 to −105	0.0127		120

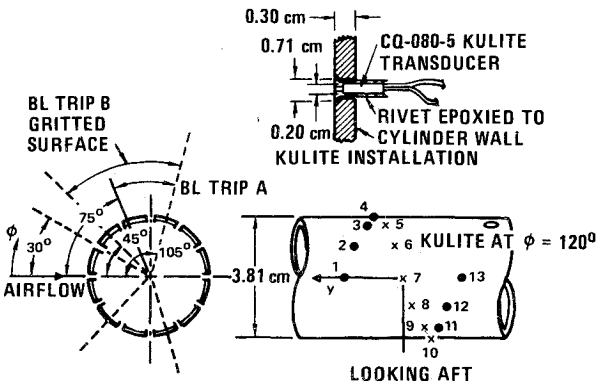

Fig. 2 Description of boundary-layer trip configurations and surface pressure instrumentation.

Aerodynamic Test Results

Figure 3 shows the variation of drag coefficient vs Mach number and Reynolds number (shown on parallel scales) for the 3.81-cm cylinder, for the various BL trip configurations, along with the published smooth cylinder data of Batham,[15] Fage and Warsap, and Weiselberger (see summaries in Refs. 14 and 8). Figure 4 shows drag coefficient data for the 1.9-cm cylinder for smooth and rough conditions. In Figs. 2 and 3 the scales of Reynolds number and Mach number are shown in parallel emphasizing their simultaneous variation with Mach number. It is known (Ref. 16, Vol. II, p. 684) that compressibility drag onset for cylinders begins to be noticeable in some tests (at $Re = 100{,}000$) at Mach numbers as low as 0.3 to 0.4. Although the local Mach numbers are still subsonic, the laminar boundary layer on the cylinder commences to separate farther forward, due to the well-known effects of compressibility on a laminar boundary layer when subjected to an adverse pressure gradient.[16] This permature laminar boundary separation due to compressibility manifests itself in an increase in pressure drag; this effect is exactly opposite to the beneficial effect of increased Reynolds number which delays boundary-layer separation on the cylinder.

The smooth cylinder drag variations from the present 3.81-cm cylinder tests had only a limited range, from $C_D = 1.2$, at subcritical Reynolds numbers, to minimum of 0.97, at 0.45 Mach number and 400,000 Reynolds number. Because of the desired and achieved turbulence level in the test section (less than 0.4% of the freestream velocity) the transition from subcritical to supercritical Reynolds number did not occur until about 270,000 Reynolds number. The drag coefficient increased abruptly again at 0.5 Mach number, due to well-known compressibility effects on drag. By contrast, the data cited in Refs. 8, 15 and 11 reached lower values of drag coefficient at higher supercritical Reynolds numbers by using larger-sized cylinders and testing at low Mach numbers. For the smooth, 1.9-cm cylinder tests, the maximum Reynolds number achieved was 225,000 at 0.5 Mach number; therefore, as expected, no reduction drag coefficient was observed. The cylinders with the BL trip did provide a significant reduction of drag coefficient, yielding a minimum value of 0.75 for the BL trip A configuration, for the 3.81-cm cylinder (see Fig. 3). For the 1.9-cm cylinder with BL trip A, a minimum value of $C_D = 0.786$ is obtained after normalizing the drag data for the 1.9-cm cylinder by the ratio of 1.2/1.35. The drag data normalization is used to facilitate correlation of acoustic and drag data between the 1.9-cm cylinder and the 3.81-cm cylinder, because for the small cylinder, subcritical drag coefficient level was measured at $C_D = 1.35$, rather than the nearly classical value $C_D = 1.2$ measured for the 3.81-cm cylinder. Because of the limited pressure tap coverage for the 1.9-cm cylinder, it is possible that the drag data are in error; therefore, normalization of the small cylinder drag data to the classical subcritical value 1.2 was felt to be necessary. The

SYMBOL	CONFIG	GRIT DIA k (cm)	BL TRIP WIDTH A (DEGREES)
——○——	SMOOTH	0	NA
——●——	REPEAT SMOOTH	0	NA
– – –□– – –	BL TRIP A	0.025	75° to 105°
– – –■– – –	BL TRIP AA	0.025	75° to 105°
– – –△– – –	BL TRIP B	0.025	45° to 105°
– – –▲– – –	BL TRIP BB	0.025	45° to 105°
——○——	SMOOTH (MACH 0.021 to 0.044? BATHAM 1973)		
————	SMOOTH (FAGE & WARSAP, 1930)		
– – – – –	SMOOTH (WEISELBERGER, 1914)		

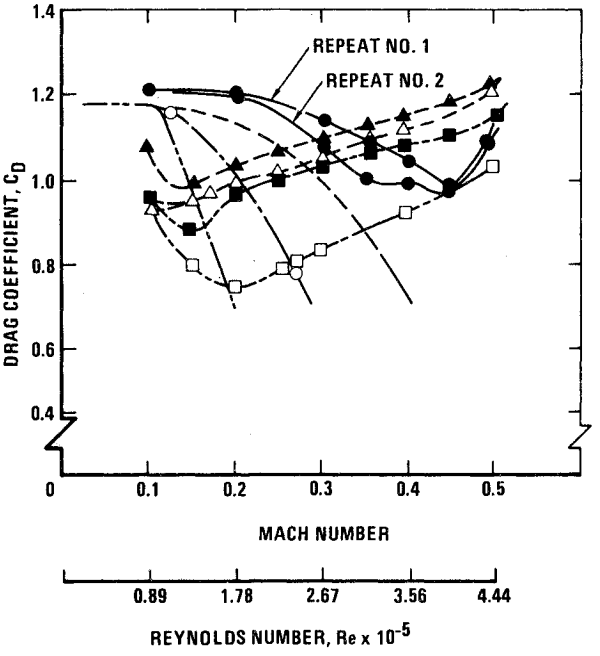

Fig. 3 Drag coefficient data summary for the 3.81-cm cylinder.

SYMBOL	BL TRIP CONFIG	METHOD OF DRAG EVALUATION
○ □	SMOOTH TRIP A	PRESSURE DRAG
▽ △	SMOOTH TRIP A	WAKE SURVEY

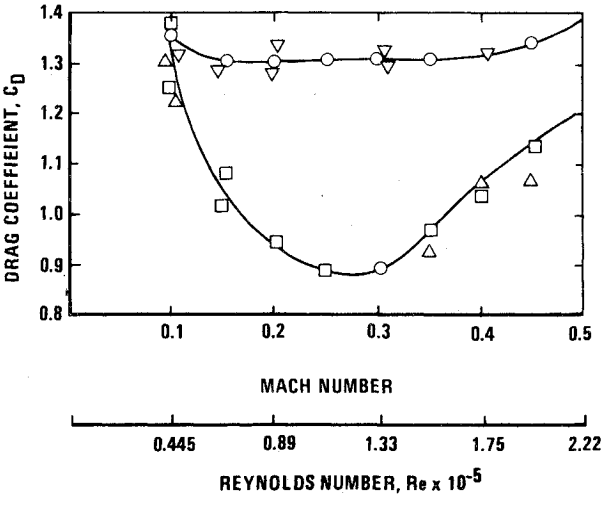

Fig. 4 Drag coefficient data summary for 1.9-cm cylinder.

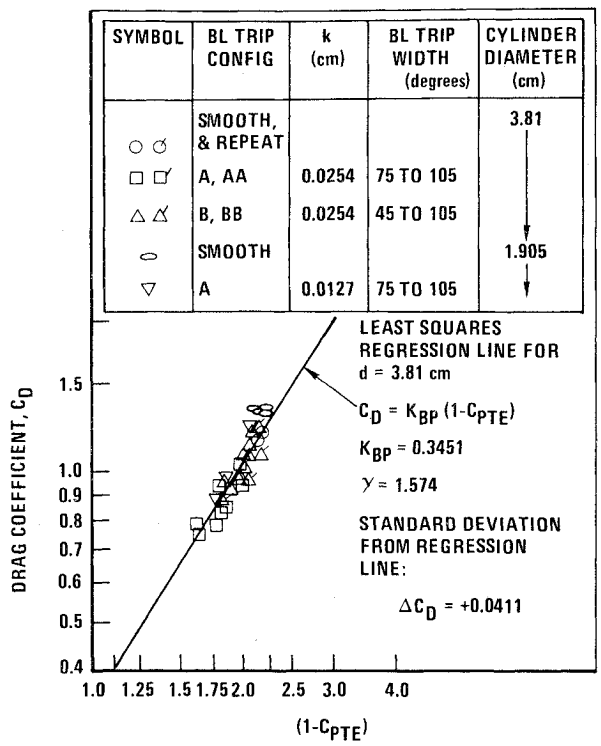

Fig. 5 Correlation of drag coefficient vs base pressure coefficient parameter.

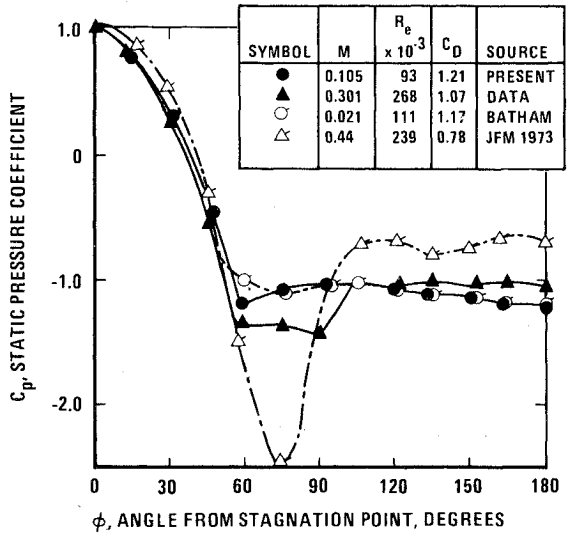

Fig. 6 Surface static pressure data.

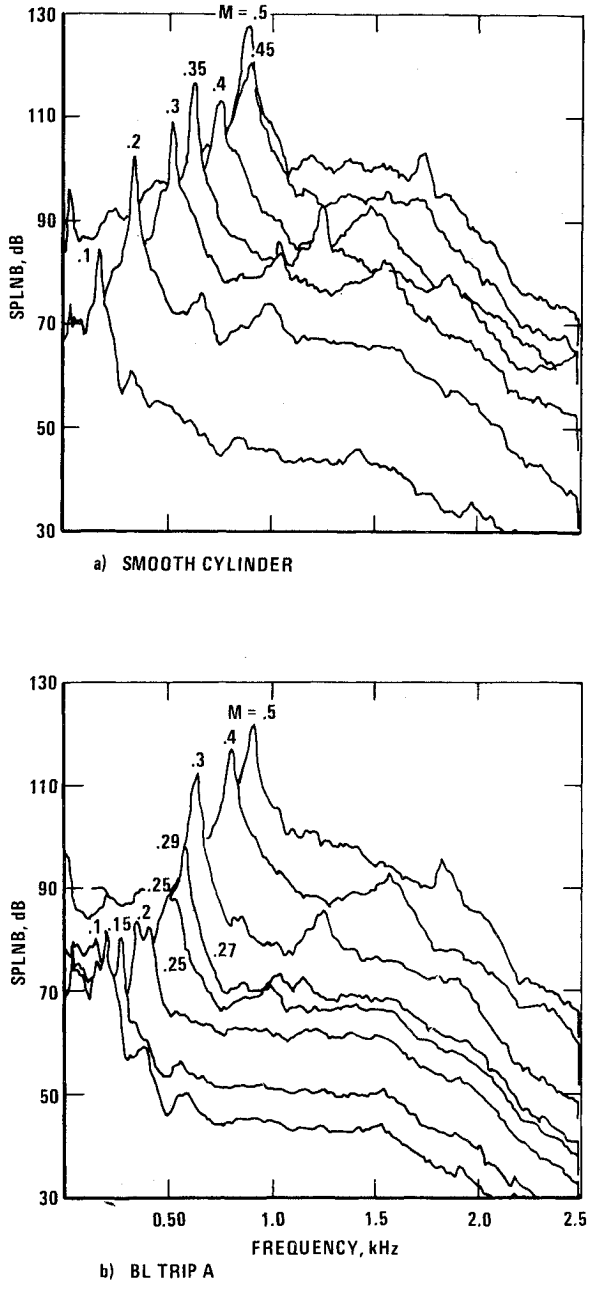

Fig. 7 Narrowband far-field SPL microphone 5, $\theta_i = 90$ deg, $r = 2.438$ m, 10-Hz bandwidth.

present pressure drag results appear in Fig. 3 to agree with wake survey results; however, it was not possible to conduct the wake survey far enough downstream to achieve a proper result, due to wind-tunnel blockage errors at the downstream wake survey plane where the potential core of the freejet is narrower than at the cylinder position. It is also noted that because of the form of Eqs. (7) and (8), multiplying C_D by a factor alters the SPL by a constant, but does not alter the coefficient of $\log_{10} C_D$; therefore, the data can be used either in the form of measured C_D or normalized C_D to deduce the slope of SPL vs $\log_{10} C_D$, which is the correlation of central interest in this paper. The normalization of the small cylinder drag data is intended to make the present correlations of SPL compatible with drag coefficient data available from other sources. For bluff bodies, it is known[13] that the pressure drag coefficient can be correlated in terms of the base pressure or trailing-edge pressure coefficient, C_{PTE}. Figure 5 shows such a correlation for the 3.81-cm cylinder. The least-squares regression curve fit to the data yields an equation, which is a particular form of Eq. (6), with $K_{BP} = 0.345$ and $\gamma = 1.574$.

Reference 7 contains detailed static pressures distributions which were also used to determine the drag coefficients reported here. Comparisons with Batham's results[16] for example (see Fig. 6), show that the static pressure distributions are in close agreement at comparable subcritical C_D values. For smooth cylinders the present tests have more negative base pressures in the range of $M = 0.2$ to 0.45 ($Re = 180{,}000$ to $400{,}000$) and the highest negative (suction) pressures near $\phi = 75$ deg are not as high as Ref. 16 at supercritical Reynolds numbers, possibly due to compressibility effects on boundary-layer separation. Figure 6 is an example showing the two effects just mentioned. Because of the weighting factor, $\cos\phi$, used in integrating the surface

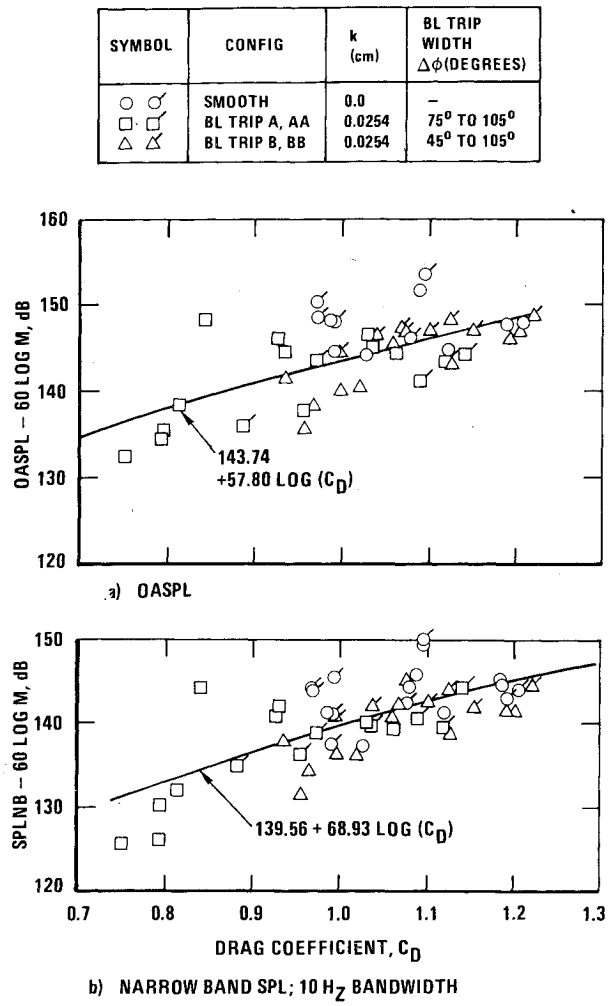

Fig. 8 Mach corrected SPL vs drag coefficient for 3.81-cm cylinder with various boundary-layer trip configurations for microphone 5, $\theta_i = 90$ deg, $r = 2.438$ m.

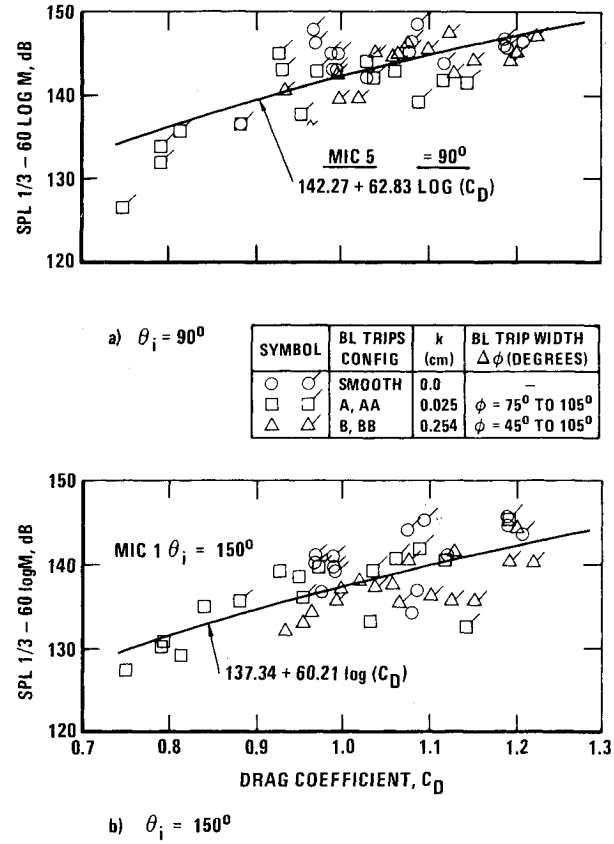

Fig. 9 Mach corrected peak one-third octave SPL vs drag coefficient for 3.81-cm cylinder, with various boundary-layer trip configurations for microphone 5, $r = 2.438$ m.

pressures to obtain the drag, the pressure coefficient differences near $\phi = 75$ deg had little effect on drag, whereas the base pressure coefficients had a large effect. The pressure drag coefficient data are estimated to be accurate within ± 0.05 for the 3.81-cm cylinder tests.

Acoustic Data and Statistical Correlation with Drag Coefficient Data

Figure 7a shows narrowband far-field SPL data for the 3.81-cm cylinder for smooth surface conditions for microphone 5, $\theta_i = 90$ deg, at $r = 2.438$ m and $r/\sqrt{bd} = 17.98$, where bd is the cross-sectional area of the cylinder. Notice the rather regular increase of the peak SPL and Strouhal frequency, except between $M = 03$ and 0.5. Figure 7b shows the narrowband SPL data for the cylinder with BL trip A, which gave the most pronounced dip in the drag coefficient vs Mach number curve. Notice especially a significant reduction of SPL near $M = 0.2$, and a tendency for tonal intermittency as indicated by the double peak. These effects on SPL are qualitatively similar to what might be anticipated theoretically from the C_D vs M data of Fig. 3.

Figures 8-10 are a small sample from the extensive graphs and tabulations of Ref. 7. Figures 8a and 8b show the Mach corrected OASPL and narrowband SPL for microphone 5, $\theta_i = 90$ deg vs drag coefficient. Figures 9a and 9b show Mach corrected peak one-third octave SPL data vs C_D, respectively, for microphones 5 and 1 at directivity angles, $\theta_i = 90$ and 150 deg.

Each of Figs. 8-10 shows the statistical, least-squares regression line of the form

$$Y_F = a_F + b_F \log_{10} C_D \tag{9}$$

The subscript F denotes far-field acoustic data. The constant a_F appears to display the primary effects of directivity and source size. The a_F values also increase in magnitude with bandwidth as is seen from Figs. 8 and 9. Conversely, the b_F coefficient, related to C_D, increases as the frequency analysis bandwidth is decreased. This is probably because the signal-to-noise ratio improves with decreasing bandwidth, especially at lower Mach numbers, and for downstream the directivity angle $\theta_i = 150$ deg (microphone 1) where the broadband noise of the freejet tunnel is higher. Figures 10a and 10b show the correlation of Mach corrected SPL vs C_D for the 1.905-cm cylinder.

Figure 11 shows the constant a_F plotted against directivity angle as determined from the large and small cylinder statistical correlations. For the 1.9-cm cylinder data, 3 dB have been added to account for the basic factor of 2 in cylinder frontal area (span times diameter). As mentioned in the aerodynamics discussion, the measured values of drag coefficient at subcritical Reynolds number were too high by a factor of 1.35/1.2; therefore, also shown in Fig. 11 are the a_F coefficient values obtained from the statistical regression of the Mach corrected SPL for the 1.9-cm cylinder vs the normalized C_D values. These are obtained by dividing the measured C_D values by the foregoing ratio. The latter curve 2 of Fig. 11 is within 3 dB of the 3.81-cm cylinder data, and an average curve 4 is suggested for prediction purposes. The directivity data of Fig. 11 are closely represented by Eq. (10).

The next topic is the statistical confidence which can be placed on these least squares coefficients, derived from the regression curves drawn through data which have a fair

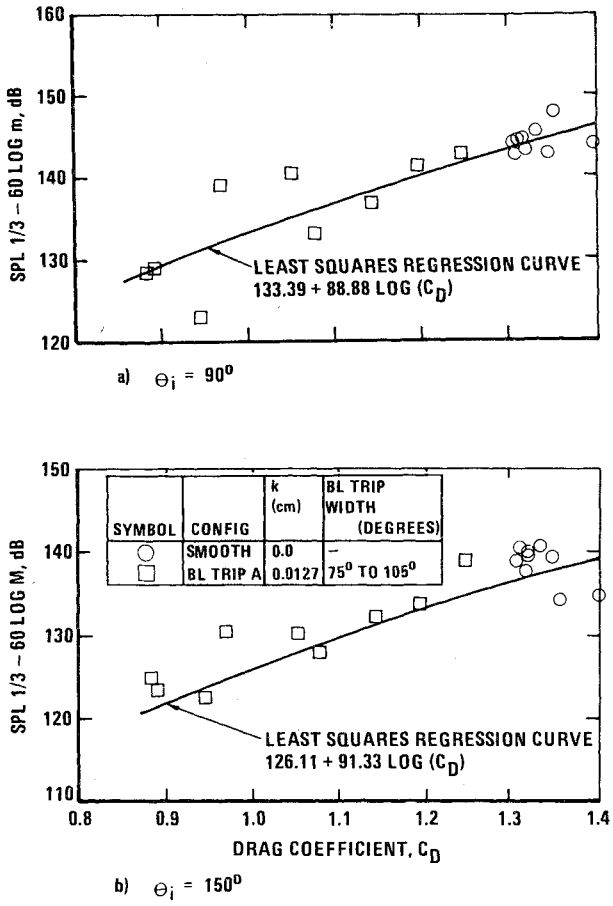

Fig. 10 Mach corrected peak one-third octave SPL vs drag coefficient for 1.905-cm cylinder with various BL trip configurations, for microphone 5, $r = 2.428$ m.

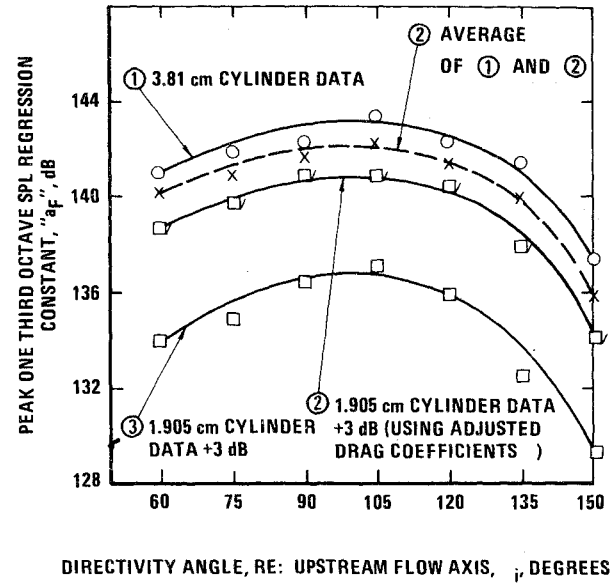

Fig. 11 Coefficient a_F from least square regression analaysis of Mach corrected peak one-third octave SPL; data adjusted to size of 3.81-cm cylinder.

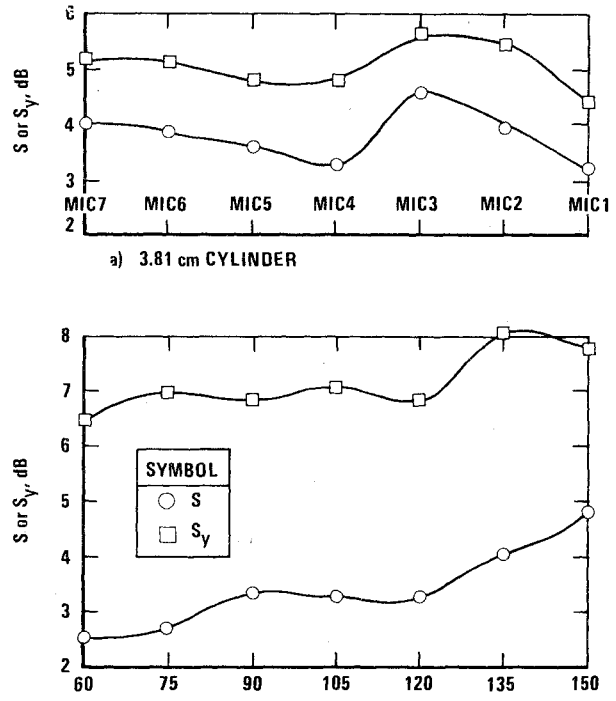

Fig. 12 Standard deviation S (from curve on Mach corrected SPL vs C_D) vs directivity angle for peak one-third octave SPL.

amount of scatter. Figures 12a and 12b show that the standard deviation S of the scatter about any of the least-squares regression curves (such as are shown in Figs. 8-10) is significantly lower than the standard deviation S_y about a horizontal line through a mean value of Y. This simple mean is the arithmetic average of the Mach corrected SPL, without regard for the supposed dependence upon C_D. Of a course the existence of a nonzero value of b_F in Eq. (9) proves the drag dependence hypothesis. Theoretically, if Y were independent of C_D, then b_F should be numerically zero; however, the comparison of S and S_y is a measure of the practical value of bothering with the attempt to correlate data in terms of C_D. Figure 12b shows that S_y is, in fact, about 4 dB worse than S for the 1.9-cm cylinder. The difference is only 1 to 2 dB for the 3.81-cm cylinder data, but still shows that a significant improvement can be achieved in prediction of noise by taking into account the drag coefficient dependence. Figure 13 shows the conventional statistical correlation coefficient R[17] for determining whether a regression equation such as Eq. (9) is statistically significant to a specified confidence level. The curves represent threshold R values required for a given confidence level as a function of the number of statistical degrees of freedom. The degrees of freedom in the present study are less than the number of test points by two, because two points (constraints) are needed to define a straight line in the logarithmic variables of Eq. (9). Figure 13 shows conclusively that the R values for the complete data sets (45 df for all of the combinations of BL trips and Mach numbers) for each of the seven microphones far exceed the threshold requirements for 99.9% confidence. In fact, the probability of no confidence is less than 10^{-4}. Also, Fig. 13 shows that from the statistical regression analyses of many of the individual BL trip data subjects, for various microphones, a high confidence level can be inferred even from these limited subset correlations with degrees of freedom as low as 5 to 7.

Figure 14 is included to test the validity of assuming a velocity to the sixth dependence (an acoustically compact dipole) as the basis for defining Mach corrected SPL. For example, if the noise mechanism were that of a quadrupole, such as is the case with jet noise,[18] one would subtract 80 $\log_{10} M$ to obtain the appropriate Mach corrected SPL, Y. Figure 14 does show that the standard deviation S from the

least-squares regression curve of Y vs $\log_{10}C_D$ is minimized if the velocity dependence exponent value selected is about 6, which is indicative of dipole noise. It is noted (not shown here) that the statistically positive correlations are obtained for the Mach corrected SPL [of the same form as Eq. (9) when 60 is replaced by $10n$ in Eq. (8)]. Figure 14 thus proves statistically that, as a mathematical model, dipole ($n=6$) is preferable to either a monopole ($n=4$) or quadrupole ($n=8$) representation.

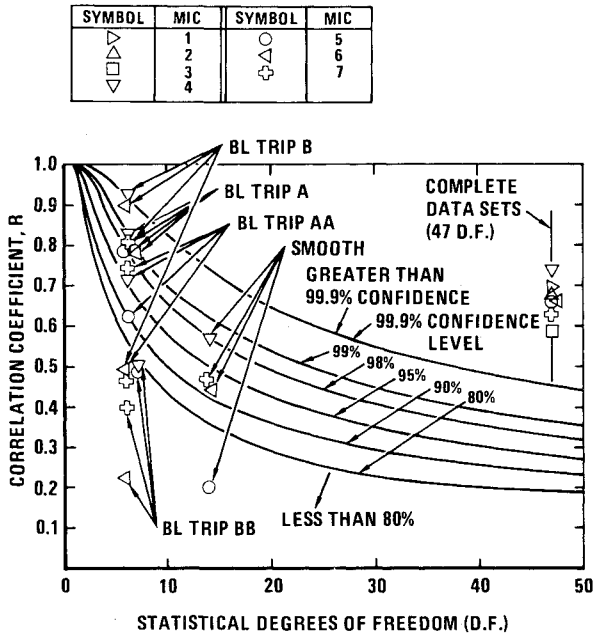

Fig. 13 Statistical confidence level test of least-square regression of Mach corrected peak one-third octave SPL vs drag coefficient for 3.81-cm cylinder.

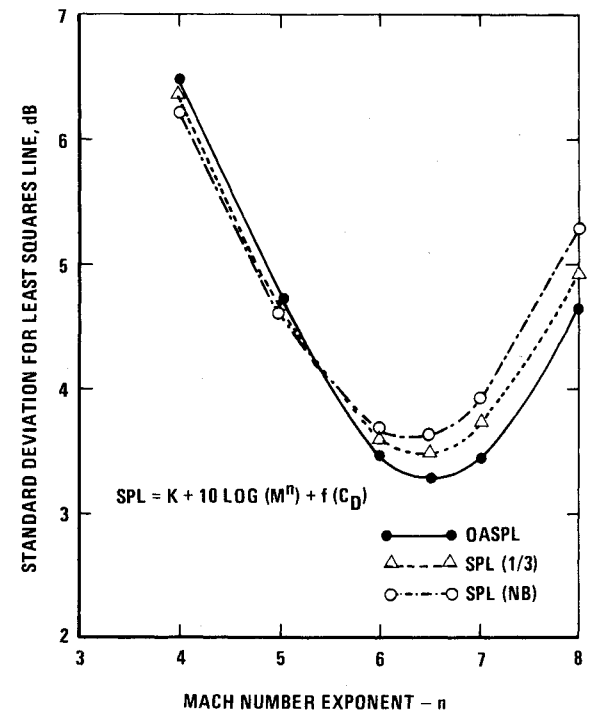

Fig. 14 Effect of assumed Mach number exponent dependence on the standard deviation of the SPL vs drag coefficient correlation of far-field noise for the 3.81-cm cylinder for microphone 5, $\theta_i = 90$ deg, $r = 2.438$ m.

Reference 7 also contains data (omitted for brevity in this paper) for surface pressure fluctuation SPL plotted as $Y_S = \text{SPL} - 40\log_{10}M$ vs $\log_{10}C_D$. The data show even stronger correlations with C_D than the far-field SPL. Reference 7 discusses the relationship between surface pressure fluctuations, and far-field SPL in some detail, and presents further refinement of the theory. Also in Ref. 7, it is shown that the surface pressure has a high degree of coherency (normalized cross spectical density) at the Strouhal frequency, with both the far-field acoustic pressure, and the hot-wire anemometer signal in the wake.

As a concluding note, Table 2 presents a summary of the best estimates of the constants a_F and b_F in Eq. (9) obtained by averaging the results for the 3.8- and 1.9-cm cylinder after adjusting the 1.9-cm cylinder data levels to those of the 3.81-cm cylinder. The results are given for a directivity angle of 90; however, values for the other angles are closely estimated by Eq. (10). Table 3 shows one-third octave average values of b_F for all seven microphones and standard deviations. The data used to generate Table 3 displayed no significant dependence of b_F on directivity angle. It can be seen from Table 2 that the levels of the a_F which measure the absolute source size increase with frequency bandwidth, while the b_F coefficient which defines the drag coefficient dependence is larger for narrower bandwidth. The bandwidths for the narrowband data are expressed as their approximate percentages of the Strouhal frequency for the 3.81- and 1.9-cm cylinders, using the fixed bandwidths of 10 Hz and 20 Hz. The last constant K_F is a preliminary value suggested for prediction purposes, when Eq. (8) is scaled to arbitrary cylinder sizes according to the following equation:

$$\text{SPL} = K_F + b_F\log_{10}C_D + 60\log_{10}M_0 + 10\log_{10}(bd/r^2) + 20\log(p_0/p_{SL}) + 10\log_{10}[(\sin\theta_i)^2 - 0.1\sin(2\theta_i) + 0.01(\cos\theta_i)^2] \quad (10)$$

The standard deviation of the directivity function is 0.78 dB for peak one-third octave band SPL data for the 3.81-cm cylinder. The reader is cautioned that this empirical equation has not been tested against any other data where both drag and far-field noise have been measured. Also, it has not been tested beyond the range $0.75 < C_D < 1.2$, and is restricted to tone dominated nonturbulent onset flows. Numerous experiments in conjunction with the study of Ref. 7 have shown that if either upstream turbulence is introduced or if the vortex wake is sufficiently disturbed by obstacles, then the strong tonal character of the noise disappears and the one-third octave SPL values will decrease by about 10 dB. It is noted from Tables 2 and 3 that the drag dependence ranges

Table 2 Best averaged values of constants a_F and b_F at $\theta_i = 90$ deg

Bandwidth	a_F, dB	b_F, dB	K_F, dB
Narrowband 6%-1%	138.0	80.3	163.1
One-third octave 26%	141.7	75.8	166.8
OASPL	143.0	72.2	168.1

Table 3 Average b_F values and standard deviation obtained from averages of all far-field measurements (seven each for 1.9- and 3.8-cm cylinders)

Cylinder diameter, cm	Bandwidth	b_F, dB	Standard deviation of b_F, dB
1.9	One-third octave	92.72	5.93
3.8		66.36	4.50
both		79.54	14.59

from 66 to 93 times $\log_{10}C_D$ compared to the theoretical 65 $\log_{10}C_D$ dependence suggested by Eq. (7). This difference is explainable in part by a stronger dependence of the surface pressure fluctuation than is indicated by the choice $\beta = 1$ in Eq. (2); however, a fuller discussion of the theory is beyond the scope of this paper. In general, the agreement between the experimental data in Table 2 and Eq. (7) is surprisingly good, which emphasizes the likelihood of a stronger dependence of bluff body noise upon drag coefficient than is predicted for streamlined bodies in Ref. 2, as discussed in the preceding theory. It is anticipated from Ref. 2 that the drag coefficient dependence must asymptotically reduce to 30 $\log_{10}C_D$ as streamline body conditions are approached; however, no studies, such as the present one are available for bodies of intermediate fineness ratio.

Conclusions

The present paper is a brief synopsis of a recent study for NASA Langley Research Center.[7] The purpose is to develop controlled laboratory test data for both far-field aerodynamic noise radiation and drag coefficient to determine if a statistically significant relationship exists. The results of Ref. 7 and this summary substantiate the SPL vs C_D relationship well beyond the 99.9% confidence level via linear regression analysis, thus substantiating the theoretical arguments of Refs. 1 and 2, as extended herein to bluff body self-generated noise.

The reader is cautioned that the impingement of upstream turbulence can alter the results considerably. In particular, the pure Strouhal tones associated with regular vortex shedding can be destroyed producing a significant reduction of peak narrowband SPL, by a modest amount of upstream turbulence of appropriate length scale. However, for non-turbulent onset flows the self noise of both smooth and rough cylinders is strongly tone dominated and well correlated with drag coefficient, in the range of 50 to 90 times $\log_{10}C_D$, over a wide range of Reynolds number and surface roughness conditions.

Acknowledgment

The authors would like to acknowledge the help of F. J. Balena, E. P. Feltz, J. L. Hayward, D. L. Morrow, B. H. Robinson, and G. W. Painter at Lockheed-California Company and D. J. Fratello, J. C. Hardin, and D. L. Lansing at the NASA Langley Research Center for their sponsorship of part of this research.

References

[1] Revell, J. D., "The Calculation of Aerodynamic Noise Generated by Large Aircraft at Landing Approach," *87th Meeting of the Acoustical Society of America*, Paper JJ9, April 1974.

[2] Revell, J. D., Healy, G. J., and Gibson, J. S., "Methods for the Prediction of Airframe Aerodynamic Noise," AIAA *Progress in Astronautics and Aeronautics—Aeroacoustics: Wave Propagation; Aircraft Noise Prediction; Aeroacoustic Instrumentation*, Vol. 46, edited by I. R. Schwartz, N.Y., 1976, pp. 139-154; also AIAA Paper 75-539, 1975.

[3] Revell, J. D., "Induced Drag Effect on Airframe Noise," AIAA *Progress in Astronautics and Aeronautics—Aerocoustics: STOL Noise, Airframe and Airfoil Noise*, Vol. 45, edited by I. R. Schwartz, N.Y., 1976; also AIAA Paper 75-487, 1975.

[4] Healy, G. J., "Aircraft Far-Field Aerodynamic Noise: Its Measurement and Prediction," AIAA *Progress in Astronautics and Aeronautics—Aerocoustics: STOL Noise, Airframe and Airfoil Noise*, Vol. 45, edited by I. R.Schwartz, N.Y., 1976, pp. 203-219; also AIAA Paper 75-486, 1975.

[5] Gibson, J. S., "Non-Engine Aerodynamic Noise Investigation of a Large Aircraft," NASA CR 2378, Oct. 1974.

[6] Lasagna, P. L. and Putnam, T. W., "Preliminary Measurements of Aircraft Aerodynamic Noise," AIAA Paper 74-572, June 1974.

[7] Revell, J. D., Prydz, R. A., and Hays, A. P., "Experimental Study of Airframe Noise vs Drag Relationship for Circular Cylinders," Lockheed-California Co., LR 28074, Feb. 25, 1977.

[8] Schlichting, H., *Boundary Layer Theory*, fourth ed., McGraw-Hill, New York, 1960.

[9] Aupperle, F. A. and Lambert, R. F., "Effects of Roughness on Measured Wall Pressure Fluctuations Beneath a Turbulent Boundary Layer," *Journal of the Acoustical Society of America*, Vol. 47, Jan. 1970, pp. 359-370.

[10] Hoerner, S. F., *Fluid Dynamic Drag*, published by author, Midland Park, Md., 1965.

[11] Revell, J. D., Prydz, R. A., and Hays, A. P., "Experimental Investigation of Aerodynamic Noise vs Drag Relationships for Circular Cylinders," AIAA Paper 77-1292, Atlanta, Ga., Oct. 1977.

[12] Kadman, Y. and Hayden, R. E., "Factors in the Design and Performance of Free-Jet Acoustic Wind Tunnels," AIAA *Progress in Astronautics and Aeronautics—Aeroacoustics: STOL Noise; Airframe and Airfoil Noise*, Vol. 45, edited by I. R. Schwartz, N.Y., 1976, pp. 247-258.

[13] Braslow, A. L., Hicks, R. M., and Harris, R. V., "Use of Grit Type Boundary Layer Transition Trips on Wind Tunnel Models," NASA TND-3579, Sept. 1966.

[14] Goldstein, S., ed., *Modern Developments in Fluid Dynamics*, Vols. I and II, Oxford University Press, 1938.

[15] Batham, J. P., "Pressure Distributions on Cylinders at Critical Reynolds Numbers," *Journal of Fluid Mechanics*, Vol. 57, Pt. 2, Feb. 1973, pp. 209-228.

[16] Howarth, L., ed., *Modern Development in Fluid Dynamics, High Speed Flow*, Vols. I and II, Oxford University Press, 1953.

[17] Volk, W., *Applied Statistics for Engineers*, McGraw-Hill, N.Y., 1958.

[18] Lighthill, M. J., "On Sound Generated Aerodynamically; I General Theory," *Proceedings of the Royal Society (London)*, Vol. A211, 1952, pp. 564-587.